

Transition-Based Constrained DFT for the Robust and Reliable Treatment of Excitations in Supramolecular Systems

Martina Stella,^{†,¶} Kritam Thapa,[†] Luigi Genovese,[‡] and Laura E. Ratcliff^{*,†,§}

[†]*Department of Materials, Imperial College London, London SW7 2AZ, United Kingdom*

[‡]*Univ. Grenoble Alpes, CEA, IRIG-MEM-L_Sim, 38000 Grenoble, France*

[¶]*The Abdus Salam International Centre for Theoretical Physics, Condensed Matter and Statistical Physics, 34151 Trieste, Italy*

[§]*Centre for Computational Chemistry, School of Chemistry, University of Bristol, Bristol BS8 1TS, United Kingdom*

E-mail: laura.ratcliff@bristol.ac.uk

Abstract

Despite the variety of available computational approaches, state-of-the-art methods for calculating excitation energies such as time-dependent density functional theory (TDDFT), are computationally demanding and thus limited to moderate system sizes. Here, we introduce a new variation of constrained DFT (CDFT), wherein the constraint corresponds to a particular transition (T), or combination of transitions, between occupied and virtual orbitals, rather than a region of the simulation space as in traditional CDFT. We compare T-CDFT with TDDFT and Δ SCF results for the low lying excited states (S_1 and T_1) of a set of gas phase acene molecules and OLED emitters, as well as with reference results from the literature. At the PBE level of theory, T-CDFT outperforms Δ SCF for both classes of molecules, while also proving to be more robust. For the local excitations seen in the acenes, T-CDFT and TDDFT perform equally well. For the charge-transfer (CT)-like excitations seen in the OLED molecules, T-CDFT also performs well, in contrast to the severe energy underestimation seen with TDDFT. In other words, T-CDFT is equally applicable to both local excitations and CT states, providing more reliable

excitation energies at a much lower computational cost than TDDFT. T-CDFT is designed for large systems and has been implemented in the linear scaling BigDFT code. It is therefore ideally suited for exploring the effects of explicit environments on excitation energies, paving the way for future simulations of excited states in complex realistic morphologies, such as those which occur in OLED materials.

1 Introduction

Studying excited states in molecules and extended systems is one of the major ongoing challenges in physics, chemistry and materials science due to the complexity of the underlying electronic structure. Nonetheless, an accurate characterization of excitation energies is crucial for a fundamental understanding of systems of technological interest, e.g. solar cells¹, organic light emitting diodes^{2,3} and chromophores in biological systems⁴. One example of interest is thermally activated delayed fluorescence (TADF) emitters, which have gained a spotlight in recent years as a new type of organic light emitting diode (OLED)^{2,3}. This is due to their promising maximum theoretical internal quantum efficiency (IQE) of 100%⁵⁻⁷. TADF

relies on a reverse intersystem crossing (RISC) mechanism (triplet-to-singlet energy up conversion, illustrated by a simplified Jablonski diagram in Fig. 1) to achieve such high efficiency without employing expensive noble metal ions. TADF is however only possible at appreciable rates if the singlet-triplet splitting, ΔE_{ST} , (defined in Fig. 1) is smaller than or comparable to $k_b T$, where k_b is the Boltzmann constant and T the temperature. Therefore, accurate prediction of ΔE_{ST} is a key but challenging element for designing more efficient TADF emitters. Excited states in TADF can be a mixture of charge transfer (CT) and local excitations (LE), while their nature can vary with both chemical structure and changes in molecular conformation⁸.

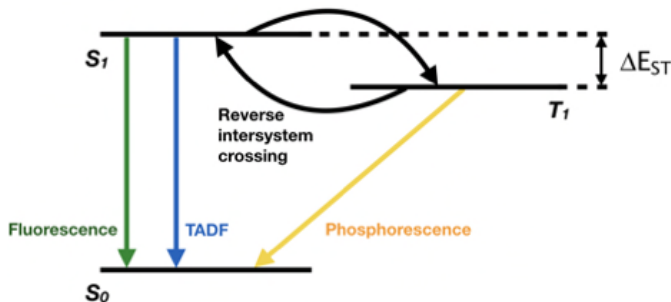


Figure 1: Simplified Jablonski diagram for TADF emitters. Reverse intersystem crossing, represented in the figure by the arrow going from T_1 to S_1 (with the intersystem crossing going from S_1 to T_1), is thermally activated when the energy difference between the two excited states is smaller or comparable to $k_b T$.

Experiments for investigating excitations can be challenging because of factors such as technical setups and short lifetimes. In addition, the classification and interpretation of the nature of different excitations (i.e. valence state, CT, LE) is often based on empirical data. *Ab initio* simulations therefore represent a valuable tool. However, as the example of TADF also highlights, there are many challenges that lie within the computational modelling of excited states, including the need to go beyond gas phase simulations and instead consider realistic morphologies⁹. In this context it is necessary to develop a methodology which is able to reliably capture the excited electronic structure, while account-

ing for both conformational and environmental effects of the full system, and still maintaining an affordable computational cost.

In this paper we present a new computational approach motivated by the desire to simulate excitations in large systems for applications such as TADF. In order to motivate our approach, we first present an overview of currently available *ab initio* approaches for excited state calculations, many of which have been developed in recent years as a result of community efforts to provide accuracy (see e.g. Ref.¹⁰) as well as precision benchmarks¹¹ for molecular quantities beyond the ground state.

1.1 Density Functional Theory-Based Methods for Simulating Excited States

Density functional theory (DFT)^{12,13} has established itself as one of the most promising approaches for studying excitations in molecules and large systems, mainly due to its notoriously favourable trade-off between accuracy and computational cost. However, it is well known that, in its standard form, DFT falls short when describing excited states because of the ground-state nature of its formulation. For this reason a range of different DFT-based methodologies have been developed in order to better account for excited electronic states.

Δ SCF (self-consistent field)¹⁴ is the simplest DFT-based approach for computing excitation energies. For a given excited state of interest the energy splitting is defined as $\Delta E_{SCF}^n = E_n - E_0$, where E_0 is the ground state energy and E_n is the energy of an “excited” state, labelled by n , which is obtained by manually controlling the occupation of the Kohn-Sham (KS) states as the system reaches self-consistency. The Δ SCF approach has been used with wide success because of its simplicity and low computational cost. It has, for a long time, been justified in cases where the excited state corresponds to the lowest state of a given symmetry¹⁵, while its applicability has been also extended, such that it gets a formal justification in the general case¹⁶.

Linear-response (LR) time-dependent DFT (TDDFT)^{17,18} is the most commonly used method for investigating excitations in molecular systems, as it often provides good agreement with experiment. Despite being well established and more affordable than sophisticated post-Hartree-Fock methods such as CCSD(T) and CASSCF¹⁹, LR-TDDFT nonetheless has limitations which prevent it from being feasibly employed in modelling realistic morphologies, such as those in which TADF emitters are employed. First, its computational cost is still too onerous for modelling systems larger than a few hundred atoms²⁰, although various approaches have been developed for treating large systems, e.g. linear scaling TDDFT²¹ and GPU-accelerated approaches²², as well as subspace-based approaches²³. Second, it notoriously fails when describing CT states with routinely used semi-local functionals^{24,25}. The latter issue in particular has been extensively studied and a number of solutions are nowadays available, of which the most successful is the use of range-separated hybrid functionals²⁶. However, such functionals are still not widely available and can make calculations more expensive, while good performance often necessitates the tuning of the functional parameters for the system in question²⁵.

Another DFT-based method for studying excited states is constrained DFT (CDFT)^{27,28}. In CDFT a constraint is added to the density, following which the energy is found by minimising the density with this additional condition. In its most common form a specific electronic charge is constrained to a region of simulation space. If opportunely guessed, such a constraint can correspond to a specific excited state where the electronic density is well localized within the region, and takes into account, *by design*, the self-consistent response of the system to the imposition of such a constraint. For this reason, CDFT has performed very successfully for molecular systems with an obvious spatial separation between donor and acceptor regions²⁸⁻³⁵. Such a simple approach naturally overcomes some of the well-known limitations of DFT, e.g. the self-interaction problem and the resulting delocalization errors, making CDFT

particularly appropriate for treating CT states and an asset for modelling exciton formation. CDFT is conceptually intuitive and follows the same scaling as DFT (generally scaling with the cube of system size). However, it is most appropriate where some information is known about the excitation in question (where and how much charge to impose). For a comprehensive review of CDFT, we refer the reader to Ref³⁶.

The simplicity of its framework has also made CDFT attractive for the development of new variations. Recently, Ramos and Pavanello^{37,38} proposed two versions of CDFT. In a first implementation³⁷ they combine CDFT with a frozen density embedding approach. The method, termed constrained subsystem DFT (CSDFE), is mainly applied to describe hole transfer reactions. In a later paper³⁸, they present a CDFT method tailored to compute low-lying electronic excitations (XCDFT) of molecular systems, which resolves the space of virtual states by projection. The results show an accuracy only slightly worse than LR-TDDFT. A more recent paper by Roychoudhury *et al.*³⁹ proposes a generalization of CDFT for charge-compensating electronic excitations in molecules (XDFT). The obtained results are again comparable to TDDFT.

Beyond the above methods, there are also other DFT-based approaches to excited state calculations, which are either generally applicable, such as orthogonality constrained DFT⁴⁰, or designed for CT states, such as constricted variational density functional theory⁴¹. In short, there are many approaches which can compute low lying excitations in molecular systems, with each displaying limitations either in the ability to describe particular classes of excited states (LE *vs.* CT), or in the maximum accessible system size.

Furthermore, beyond the ability to treat many atoms, the complexity of large systems often also necessitates the ability to map to local degrees of freedom (DoF)^{42,43}. To this end, it would be highly advantageous to have an excited state method which can be related to a local description of a large system, e.g. to excite a single molecule within a cluster of molecules. Given all these factors, there is no clear consen-

sus on the best approach to use, particularly for applications such as TADF where the nature of the excitation can be a combination of LE and CT, and the effect of an extended environment can be crucial for accurately describing the excitation. Nonetheless, the recent variants of CDFT demonstrate its potential for providing accurate results with a lower computational cost than TDDFT.

In this paper we present an alternative variation of CDFT. In our approach, which is implemented in the wavelet-based BigDFT code⁴⁴, the constraint is defined as a particular *transition*, or combination of transitions, between given occupied and virtual states, rather than a region of the simulation space. The approach is therefore termed transition-based CDFT (T-CDFT). The transition constraint takes inspiration from an optical excitation term, rigorously defined from LR equations and parameterized for instance from LR-TDDFT. In this context, it can be considered as a further step beyond LR calculations, where SCF effects are added *on top* of the optical excitation. We consider both ‘pure’ transitions between one occupied molecular orbital (the highest occupied molecular orbital) and a single orbital in the unoccupied sector – which require no additional simulation input – as well as ‘mixed’ excitations involving more than one occupied \rightarrow virtual transition, where we use TDDFT to define the transition breakdown. We benchmark our approach on low lying singlet and triplet excitations of a set of molecules in gas phase, including both acenes and OLED emitters, putting the results in comparison with Δ SCF and TDDFT calculations. While the present work focuses on gas phase simulations, we also describe a path towards future large scale simulations, using the ability of BigDFT to treat systems containing thousands of atoms^{45,46}.

The outline is as follows. In Section 2 we first present the underlying formalism of T-CDFT, before describing the implementation in BigDFT. We finish Section 2 by defining two indicators which will be used for analyzing excitations, and specifying the computational details. In Section 3 we present the results, first discussing the nature of the excitations, including

both LE/CT character and the effect of treating excitations as pure or mixed. We finish with a detailed comparison between the obtained excitation energies for the different methods, for both LE and CT excitations. Finally, in Section 4, we conclude.

2 Methods

2.1 Excitations in the Linear-Response Formalism

When a system is submitted to an excitation, its density matrix, and therefore its observables, are modified by the effect of a (potentially frequency-dependent) perturbing operator $\hat{\Phi}(\omega)$, with ω being the frequency. Stated otherwise, we can identify a response density operator $\hat{\rho}'(\omega)$ which represents the deviation of the density matrix from the ground-state equivalent, indicated by $\hat{\rho}_0$. Such a response density satisfies an equation of motion written in the form of a quantum Liouville (super) operator, $\hat{\mathcal{L}}$, (see for example Ref.⁴⁷):

$$(\omega - \hat{\mathcal{L}}) \hat{\rho}'_{\Phi}(\omega) = [\hat{\Phi}(\omega), \hat{\rho}_0] . \quad (1)$$

Its action on a generic operator \hat{O} reads

$$\hat{\mathcal{L}}\hat{O} \equiv [\hat{H}_0, \hat{O}] + [\hat{V}'[\hat{O}], \hat{\rho}_0] , \quad (2)$$

where \hat{H}_0 is the ground-state Hamiltonian and $\hat{V}'[\hat{O}] \equiv \int d\mathbf{r}d\mathbf{r}' \frac{\delta \hat{V}[\hat{\rho}_0]}{\delta \rho(\mathbf{r}, \mathbf{r}')} O(\mathbf{r}, \mathbf{r}')$ encodes the response of the $\hat{\rho}$ -dependent potential to a modification of the density operator. The “excitation modes” of the molecule are defined through the *excitation operators* \hat{E}_a , satisfying

$$\hat{\mathcal{L}}\hat{E}_a = \Omega_a \hat{E}_a , \quad (3)$$

with Ω_a being the excitation energies. The operator orthonormalization condition

$$\text{Tr} \left(\hat{E}_a \hat{E}_b \right) = \delta_{ab} , \quad (4)$$

where \hat{E}_a is the excitation operator associated to the left Liouvillian eigenproblem⁴⁸, guaran-

tees that the excitation operators can be seen as a basis for representing the perturbation of the system.

Under a linear-response condition, it is possible to show⁴⁸ that the excitation operators satisfy the so-called *transverse* condition, which states that

$$\left(\hat{E}_a\right)_\perp \equiv \hat{\rho}_0 \hat{E}_a \hat{Q}_0 + \hat{Q}_0 \hat{E}_a \hat{\rho}_0 = \hat{E}_a, \quad (5)$$

where $\hat{Q}_0 = \hat{\mathbb{I}} - \hat{\rho}_0$ is the projector to the empty subspace of the ground-state Hamiltonian \hat{H}_0 . According to this condition, excitation operators can be parametrized as

$$\hat{E}_a = \sum_p \left(|\phi_p^a\rangle \langle \psi_p| + |\psi_p\rangle \langle \chi_p^a| \right). \quad (6)$$

We here indicate as ψ_p the occupied orbitals, where ϕ_p^a and χ_p^a are associated to vectors belonging to the span of unoccupied states (and are therefore orthogonal to the set of all occupied orbitals).

Each excitation mode of the system, with associated energy Ω_a , is thus described by a set of states $\{\phi_p^a, \chi_p^a\}$, each defined in the unoccupied subspace. It is possible to show⁴⁸ that these objects represent, respectively, the state into which $|\psi_p\rangle$ is excited – or from which it decays – when the system is subject to the *monochromatic* perturbation $\hat{\Phi}_a \equiv [\hat{E}_a, \hat{\rho}_0]$, which would only resonate with the excitation having an energy Ω_a (see⁴⁸). The spectrum is symmetric with respect to the inversion of the eigenvalues $\Omega_a \rightarrow -\Omega_a$ and, given a specific excitation $\{\phi_p^a, \chi_p^a\}$, the associated solution with opposite energy is described by the transposed pair $\{\chi_p^a, \phi_p^a\}$.

2.2 Transition-Based Constrained DFT

Excited states, as calculated for example with LR-TDDFT, may be characterized by the orbitals involved in a given transition. Each of the occupied orbitals labelled by ψ_p is then associated with a particular transition of this state in the unoccupied sector.

Following these guidelines, we define the (Her-

mitian) transition operator, \hat{T}_a :

$$\begin{aligned} \hat{T}_a &\equiv \frac{1}{\sqrt{2}} \left(\hat{E}_a + \hat{E}_a^t \right) = \\ &= \sum_p \frac{1}{\sqrt{2}} \left(|w_p^a\rangle \langle \psi_p| + |\psi_p\rangle \langle w_p^a| \right), \quad (7) \end{aligned}$$

which is associated with the linear combination of an excitation and a de-excitation with the same energy. Normalization of the excitation modes implies that $\sum_p \langle w_p^a | w_p^a \rangle = 1$. A representation of the states $|w_p^a\rangle \equiv |\phi_p^a\rangle + |\chi_p^a\rangle$ can be provided by introducing an explicit basis $\{|s\rangle\}$ in the subspace of empty states so that both $|\phi_p^a\rangle$ and $\langle \chi_p^a|$ can be represented as

$$|w_p^a\rangle = \sum_s W_{ps}^a |s\rangle. \quad (8)$$

The representation of the above equation in the basis set of the eigenvalues of the ground-state Hamiltonian gives rise to the TDDFT Casida's equations. For semi-local DFT functionals, the normalized coefficients W_{ps}^a can be directly extracted from the Casida's coupling matrix eigenproblem, thereby providing an explicit representation of $|w_p^a\rangle$.

We define our excitation energies *via* the following:

$$E_{\text{T-CDFDFT}}^{(a)} \equiv E[\rho] \Big|_{\text{Tr}(\hat{\rho}\hat{T}_a)=1} - E[\rho_0], \quad (9)$$

where we denote by $E[\rho]$ the SCF energy obtained from the density ρ . In other terms, we minimize the energy by imposing self-consistency under the transition constraint imposed by the operator \hat{T}_a . More specifically, the density matrix operator is constrained such as to include the transitions $\psi_p \rightarrow w_p^a$ in its definition. The energy of the system is then minimized along the set of solutions implementing such a constraint.

2.2.1 Transition Breakdown

We now describe the procedure for imposing the constraint onto the density. A particular excitation (labelled by a) is characterized by the set

of occupied states $|\psi_p\rangle$ which are excited into the corresponding unoccupied orbitals $|s\rangle$ with a weight provided by the coefficients W_{ps}^a . This may involve only one occupied p orbital, e.g. the highest occupied molecular orbital (HOMO), or it may involve a mixture of several orbitals. We refer to the former as a ‘pure’ transition, while the latter is considered a ‘mixed’ transition. For a given orbital p the level of purity of the transition a can be quantified by means of a transition purity indicator, \mathcal{P}_p^a , defined as

$$\mathcal{P}_p^a \equiv \langle w_p^a | w_p^a \rangle ; \quad (10)$$

which would lead to a value of one if only the orbital ψ_p participates in the transition. Clearly $\sum_p \mathcal{P}_p^a = 1$ for any excitation a .

For the generic case of a mixed transition, it is then enough to split the T-CDFT approach into multiple constraints: by decomposing the transition \hat{T}_a into partial terms:

$$\hat{T}_a = \sum_p \hat{T}_p^{(a)} , \quad (11)$$

where $\hat{T}_p^{(a)}$ is a pure transition defined from the sole ket $|w_p^a\rangle$, we can define the energy of the mixed transition by the SCF energy obtained from the density operator

$$\hat{\rho}^a = \sum_p \mathcal{P}_p^a \hat{\rho}_p^a , \quad (12)$$

where $\hat{\rho}_p^a$ is the SCF density obtained from the pure T-CDFT calculation with the constraint $\text{Tr}(\hat{\rho}_p^{(a)}) = 1$.

2.2.2 Extracting Singlet and Triplet Excitations

With this representation, the orbital sector of the configuration interaction space is, by construction, identical between up and down spins. Therefore, spin-contamination is forbidden, and we work in the subspace of $S_z = 0$ excitations. Singlet (+) and triplet (−) transitions can be easily identified, taking the solutions with $W_{ps\uparrow}^a = \pm W_{ps\downarrow}^a$, respectively.

In the KS DFT formalism, $\hat{\rho}_0$ is found by SCF

optimization of the following Lagrangian:

$$E_{BS} = \text{Tr} \left(\hat{H}_{\text{KS}}[\hat{\rho}]\hat{\rho} \right) , \quad (13)$$

where the KS Hamiltonian H_{KS} is functionally dependent on the density matrix. To impose the constraint we may add to the above Lagrangian the following term

$$C_a = \sum_{p,s} V_a^{ps} (\langle s | \hat{\rho} | \psi_p \rangle - W_{ps}^a) . \quad (14)$$

The set of Lagrange multipliers $V_c^{s,s'}$ is there to enforce the condition

$$\begin{aligned} \text{Tr} \left(\hat{\rho} \hat{T}_a \right) &= \sum_{p,s} (W_{ps}^a \langle s | \hat{\rho} | \psi_p \rangle) = \\ &= \sum_p \langle w_p^a | \hat{\rho} | \psi_p \rangle = 1 \end{aligned} \quad (15)$$

which would add to the KS Hamiltonian a density-independent term:

$$\hat{H}_c^a = \sum_{p,s} V_a^{ps} (|\psi_p\rangle \langle s| + |s\rangle \langle \psi_p|) , \quad (16)$$

where the sum should only be performed on the set of states p, s such that $W_{ps}^a \neq 0$. Once the appropriate values for the Lagrange multipliers are found, the energy of the excited system can be calculated with the usual KS expression, after removing the constraining term from H_{KS} . Singlet and triplet transitions can then be associated with constraint operators which are spin-averaged (+) and spin-opposite (−), respectively: ($\hat{H}_c^{a\uparrow} = \pm \hat{H}_c^{a\downarrow}$).

Such a formalism is particularly practical because for each pure transition $\hat{T}_p^{(a)}$, one can choose an arbitrarily large Lagrange multiplier, as the representability condition of the density matrix will always guarantee $\langle w_p^a | \hat{\rho} | \psi_p \rangle \leq 1$. A value of a magnitude of 20 atomic units for V_c is largely sufficient for imposing the constraint, as discussed in Section 2.5. Therefore, although the computational cost increases with the number of components in a given mixed excitation, the overall cost is comparable to traditional CDFT, where several calculations may be required to identify the Lagrange multiplier which satisfies the constraint.

2.3 Indicators for Analyzing Excitations

When analyzing excited states, it is useful to employ quantitative indicators which allow the comparison of various features of a given excitation. This includes the orbitals involved in a given transition, and the spatial character. To this end, we define the following two simple indicators.

2.3.1 Transition Purity

Both the transition purity indicator, \mathcal{P} (Eq. 10), and the T-CDFT formalism may be applied to any transition. In this work, a $\mathcal{P} = 1$ refers to a pure HOMO-virtual excitation, while a number significantly below 1 indicates that excitations involving deeper occupied orbitals have a non-negligible contribution to the overall description of the excitation.

2.3.2 Spatial Overlap

The accuracy of computed excitation energies strongly depends on whether the chosen method is able to correctly capture the character of the excitation. As discussed, this is particularly true for TDDFT, where energies of low-lying CT states calculated with some functionals may be severely underestimated, in some cases by several eV, while other functionals agree well with experiment⁴⁹. This has motivated the development of diagnostic tools for predicting the accuracy of TDDFT in a given case by classifying the nature of the excitation. It is not straightforward to develop a unique and effective descriptor, so that several examples of such developments can be found in the literature⁵⁰⁻⁵⁴. These generally include geometric descriptors based on the molecular orbitals and electron densities.

One such descriptor is the Λ -index^{54,55}, which is based on the overlap of molecular orbital moduli, and is defined as

$$\Lambda^a = \sum_{ps} W_{ps}^{a,2} \int |\psi_s(\mathbf{r})| |\psi_p(\mathbf{r})| \, d\mathbf{r}. \quad (17)$$

It has been suggested that a small orbital over-

lap, defined by a Λ value below 0.3-0.4, depending on the functional, corresponds to a CT transition which is not correctly described by TDDFT⁵⁵.

While it is possible to define indicators such as Λ which depend on the output of the excited state calculation, in this work we instead employ a simplified descriptor which is based on the particular transition that is used as the constraint in T-CDFT, i.e. the simulation input, rather than the output. For the case of pure HOMO-LUMO (lowest unoccupied molecular orbital) transitions, this results in a simplified version of the Λ -index. This descriptor, which we denote Λ_T , is based on the square root of the product of the overlap of solely the HOMO and LUMO wavefunctions and thus describes their *spatial overlap*:

$$\Lambda_T = \int |\psi_{\text{HOMO}}(\mathbf{r})| |\psi_{\text{LUMO}}(\mathbf{r})| \, d\mathbf{r}. \quad (18)$$

At the two extremes, a value of zero indicates no spatial overlap between the HOMO and LUMO, and hence a CT excitation, while a value of one represents full spatial overlap, corresponding to a LE state. We note that Λ_T does not distinguish between singlet or triplet excitations, nor does it take into account additional contributions in the case of mixed excitations. For work requiring an in-depth analysis of a particular excitation, a modified version based on the output of T-CDFT, or other indicators such as those referenced above would therefore be more appropriate.

2.4 Implementation in BigDFT

We have implemented T-CDFT in the BigDFT code⁴⁴, which uses a Daubechies wavelet basis⁵⁶. By taking advantage of the orthogonality, compact support and smoothness of wavelets, and in conjunction with accurate analytic pseudopotentials (PSPs), BigDFT is able to yield a high, systematically controllable precision. It has both a standard cubic scaling approach with respect to the number of atoms⁵⁷, and a linear scaling (LS) algorithm which can treat thousands of atoms^{45,46}. The T-CDFT imple-

mentation builds on the existing CDFT implementation in LS-BigDFT^{58,59}, wherein a support function (or wavefunction) basis is constructed for the ground state, then used as a fixed basis for the (T-)CDFT calculation. In the following we therefore first summarize the support function (SF)-based approach employed in LS-BigDFT. We then describe the generation of both SF and extended KS wavefunction basis sets, where the latter is used to verify the suitability of the SF basis for excited states.

2.4.1 Linear Scaling BigDFT

In LS-BigDFT the extended KS orbitals are expressed in terms of a set of localized SFs, ϕ_α , *via* the coefficients c_i^α ,

$$|\psi_i\rangle = \sum_{\alpha} c_i^\alpha |\phi_\alpha\rangle. \quad (19)$$

The density matrix, $\hat{\rho}$, is then defined in terms of the SFs and the density kernel, $K^{\alpha\beta}$ ⁶⁰,

$$\hat{\rho} = \sum_{\alpha\beta} |\phi_\alpha\rangle K^{\alpha\beta} \langle\phi_\beta|. \quad (20)$$

By taking advantage of the well known near-sightedness principle^{60,61}, it is possible to impose strict localization on both the SFs and density kernel. In BigDFT, the SFs are represented in the underlying wavelet basis set and optimized *in situ* during the self-consistency cycle. This results in a set of localized SFs which have adapted to their local chemical environment, giving a minimal basis which, by construction, can represent the occupied KS orbitals. Since the SFs are truncated within a user-defined localization radius, R_{loc} , systematic convergence is possible by increasing the localization radius.

The density kernel is then also optimized, either by means of the Fermi Operator Expansion (FOE)^{62,63} approach, which works directly with the density kernel, or with direct minimization or diagonalization approaches, which are used to obtain the coefficients c_i^α , from which the kernel can then be constructed. FOE used in conjunction with sparse matrix algebra, as implemented in the CheSS library⁴², results in LS

computational cost.

The localized SFs of LS-BigDFT can also be used as a means for further reducing the complexity of calculations of large systems. This is achieved *via* a fragment-based analysis, in which the system is divided into subsystems, and can be used both to reduce the computational cost by exploiting similarity between fragments^{58,64}, and to identify independent fragments and analyze interactions between them^{43,65}. SF-based T-CDFT is fully compatible with these fragment-based approaches; future work will aim at exploiting this to study excitations in environments.

2.4.2 Support Function Basis

The use of a transition-based constraint relies on the ability to accurately represent both the occupied orbitals and the virtual orbital(s) involved in the constraint. The SFs are optimized to describe the occupied states, however, as in the ONETEP code⁶⁶, which uses a similar approach to optimize the basis of non-orthogonal generalized Wannier functions (NGWFs), the unoccupied states can be poorly represented^{67,68}. In ONETEP this problem is overcome by using a projection operator to optimize a second set of NGWFs to represent the virtual states, which are then combined with the ground state NGWFs⁶⁸.

In LS-BigDFT we instead retain a single set of SFs, exploiting the direct minimization approach to optimize select virtual states alongside the occupied states⁴⁵. When only a few virtual states are required, this may be done in a single calculation. However, when a larger number of virtual states are required, it is more stable to employ a two-step approach:

1. Ground state calculation for occupied states only, to obtain the density, and an initial guess for both the SFs and kernel.
2. Non-self-consistent calculation in which the SFs and kernel are further optimized to represent a number of virtual states.

While step 1 may employ any approach to kernel optimization, step 2 requires the use of the

direct minimization approach. Since the virtual states are more delocalized than the occupied states, particularly in the case unbound of states, it is typically necessary to use larger localization radii, while depending on the nature of the virtual states, it may also be necessary to increase the number of SFs.

2.4.3 Wavefunction Basis

In order to validate T-CDFT with a SF basis, we have also employed a wavefunction (WFN)-based approach, wherein the basis set is generated *via* a ground state cubic scaling calculation with a (large) number of virtual states. These wavefunctions are then used for T-CDFT, treating them as a fixed SF basis with effectively infinite localization radii. By increasing the number of virtual wavefunctions, it is possible to systematically approach the complete basis set limit, assuming that the set of excited states w_p^a is localized (which is always true for excitations below a given threshold, see⁴⁸). Such an approach is therefore possible for comparing the choice of the excitation operator in different computational setups.

2.5 Computational Details

Vertical singlet and triplet excitations were calculated using T-CDFT, Δ SCF and TDDFT. T-CDFT calculations used PBE⁶⁹ only, as hybrid functionals are not available in LS-BigDFT, while Δ SCF and TDDFT calculations used both PBE and PBE0⁷⁰. Since T-CDFT is targeted at large systems, where hybrid functionals are often prohibitively expensive, this reflects the computational setup which would be used at scale. All ground state calculations and singlet T-CDFT calculations are spin restricted, while the remainder of the excited state calculations are unrestricted.

Δ SCF energies and the spatial overlap parameter were calculated using cubic-scaling BigDFT, where excited state calculations used the ground state wavefunctions as an initial guess to avoid convergence onto local minima, as described in the Supporting Information. The Δ SCF procedure notoriously models the

non-Aufbau electronic singlet state which is not a spin eigenfunction⁷¹. To obtain the energy of the singlet excited state, we therefore applied the common spin purification formula to the uncorrected mixed state energy $E_{S_1}^{\text{purified}}$,

$$E_{S_1}^{\text{purified}} = 2E_{S_1}^{\text{unpurified}} - E_{T_1}. \quad (21)$$

All reported S_1 Δ SCF energies are $E_{S_1}^{\text{purified}}$.

TDDFT calculations employed NWChem⁷² using the Tamm-Dancoff approximation (TDA)⁷³, with a cc-pVTZ basis set⁷⁴. LR-TDDFT calculations were also performed using BigDFT, using the full Casida formalism¹⁸, in order to determine the transition breakdown and purity. As only LDA⁷⁵ is available for TDDFT in BigDFT, these calculations, including the transition breakdowns, were performed using LDA with a WFN basis generated using PBE; the difference compared to using a basis generated with LDA was found to be negligible. T-CDFT calculations employed a SF basis with 4/9/9 SFs for H/C/N with $R_{\text{loc}} = 4.23 \text{ \AA}$; the calculated values were found to be within 0.05 eV of the converged WFN-based results, demonstrating that the SF basis is complete enough to allow accurate fixed-basis T-CDFT calculations, providing the virtual states of interest are well represented. A Lagrange multiplier of -20 was used for all T-CDFT calculations, as this was found to be large enough to converge $\text{Tr}(\mathbf{KW})$ – an example convergence plot is shown in the Supporting Information, alongside further computational details.

3 Results

Benchmark calculations of the lowest energy singlet and triplet (S_1 and T_1) excitations were performed for a set of molecules which were chosen to provide a range of LE, CT and mixed LE-CT character excitations. The test set, which is depicted in Fig. 2, consists of five acenes, namely naphthalene, anthracene, tetracene, pentacene and hexacene, which constitute a set of well characterized molecules; and four exemplar OLED molecules, namely NPh_3 (triphenylamine), 2CzPN

(1,2-bis(carbazol-9-yl)-4,5-dicyanobenzene), ACRFLCN (10-phenyl-10H-spiro(acridine-9,9'-fluorene)-2,7-dicarbonitrile) and CBP (4,4'-Bis(N-carbazolyl)-1,1'-biphenyl). NPh₃, 2CzPN and ACRFLCN are among the most investigated TADF emitters while CBP is a host molecule used to sensitize TADF emitters⁷⁶.

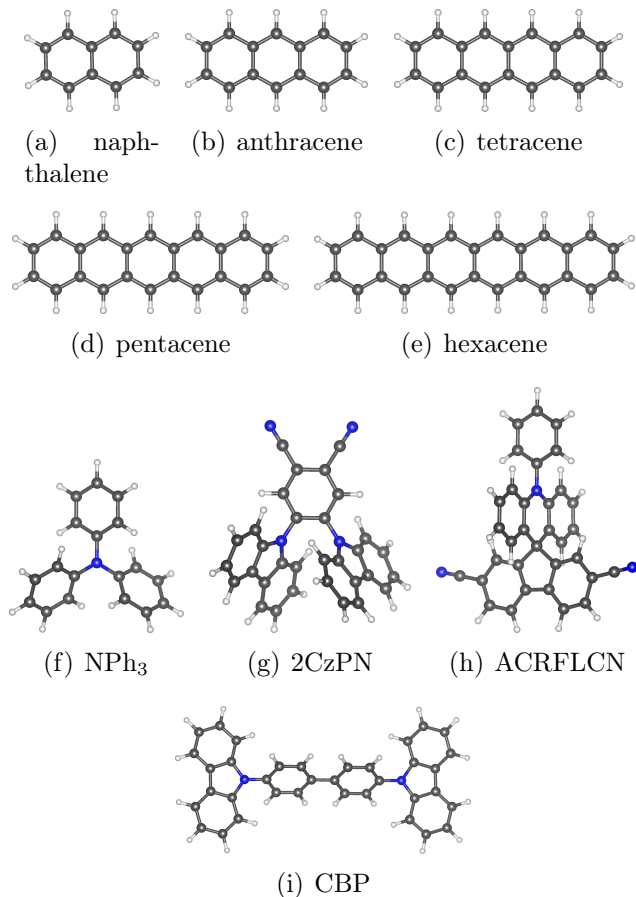


Figure 2: Relaxed atomic structures of the test set molecules. H/C/N atoms are depicted in white/black/blue.

While experimental data for these systems is available, these are typically adiabatic excitation energies, which can differ significantly from vertical excitation energies (see e.g. Ref.⁷⁷). Furthermore, such experiments take place in various external conditions, with the results being sensitive to the external environment (i.e. the solvent or other molecular environment) as well as temperature^{78,79}. As the aim of this work is to assess the performance of T-CDFT for vertical excitations in gas phase, it is therefore not informative to make quantitative comparisons with experimental data. Indeed, one

of the motivations behind this work is to provide a formalism which can treat large enough systems to take into account explicit environmental effects. Such comparisons are therefore saved for future work, while in the following we focus on theoretical comparisons only.

3.1 Nature of the Excitations

Before discussing the excitation energies, we first characterize the electronic excitations and component transitions for the benchmark molecules. The frontier orbitals for PBE are depicted in Fig. 3, alongside \mathcal{P} and Λ_T values. The equivalent PBE0 plot and the corresponding frontier orbital energies can be found in the Supporting Information.

3.1.1 Transition Purity

The HOMO-LUMO transition purity values, \mathcal{P} , show that, within our computational set up, S₁ excitations are less pure than T₁, with the least pure excitation being 0.99 for T₁ and 0.93 for S₁. We therefore expect that a HOMO-LUMO constraint in T-CDFT should represent a reasonable approximation for these molecules; in order to test this we treat the S₁ excitations of the acenes as both pure and mixed. For the mixed excitations, the transition breakdown was taken from TDDFT, neglecting all contributions smaller than 0.01, and renormalizing the transition breakdown accordingly. The results are given in Table 1. For naphthalene, which has the least pure excitation (0.93 before normalization), the energy for the mixed excitation is around 0.1 eV higher than the pure case. Whereas the mixed excitation energy for hexacene (0.98 purity before normalization), is only 0.02 eV higher than the pure excitation energy. For other excitations which are much less pure than naphthalene, the mixed nature of the excitations may have a much stronger effect on the calculated energies, although this will also vary depending on the involved transitions and not just the relative contributions. For the purposes of this work, however, these results suggest that a purity of 0.97-0.98 or above is such that neglecting other contributions should

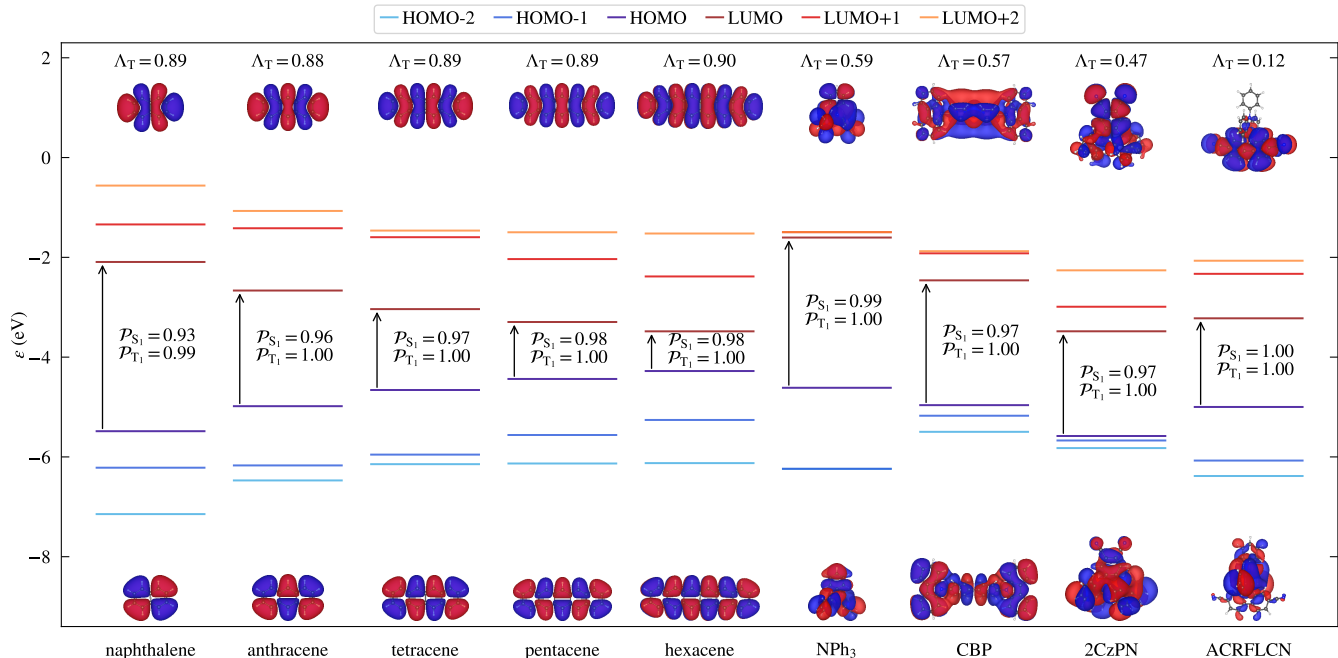


Figure 3: PBE-calculated frontier orbital energies and corresponding HOMO and LUMO wavefunctions, as obtained from cubic scaling BigDFT. Wavefunctions were visualized in VESTA⁸⁰, using an isosurface value of $0.0005 a_0^{-3/2}$. The corresponding charge transfer parameter, Λ_T and HOMO-LUMO transition purity values, \mathcal{P} , are also given for each molecule, where the latter are calculated using LDA with a PBE basis, as described in the text.

make little difference to the results. Therefore, all OLED excitations are treated as pure, while the acene results in the following are those for the mixed excitations.

3.1.2 Spatial Overlap

The high value of Λ_T for the acenes implies a strong spatial overlap between the HOMO and LUMO. Although this does not take into account the slightly mixed nature of the S_1 excitations in the shorter acenes, as a first approximation it implies that the transition constraint is local in nature, and will give rise to a predominantly local excitation (for both functionals). On the other hand, the OLED molecules have a smaller spatial overlap, so that the transition constraint and thus the excitation display a hybrid LE/CT nature of varying degrees, in agreement with previous results⁹. We therefore expect TDDFT with PBE to perform more robustly for the acenes, whereas the CT character found in the OLED excitations could lead to a less accurate description.

3.2 Acenes

We first consider the acenes, comparing our benchmark results with higher level theory calculations based on CCSD(T), which is often regarded as the gold standard of chemical accuracy in quantum chemistry⁸¹. We employ the values from Ref⁸² (and references within). The low-lying singlet excitations in the acenes are termed 1L_a and 1L_b , which differ in energetic ordering depending on the acene in question^{82,83}. However, since the 1L_a state primarily involves a HOMO-LUMO transition and thus has the same character as our calculations, we take the 1L_a values as our reference, irrespective of whether the CCSD(T)-calculated 1L_b state is lower in energy. As shown in Fig. 4, both T-CDFD and TDDFT with PBE capture the CCSD(T) trend in S_1 and T_1 energies, albeit with a systematic underestimation of both states, which increases slightly with the number of rings. This underestimation is common to all the DFT-based approaches (see Supporting Information for tabulated results).

Fig. 5(a) shows the mean absolute deviation

Table 1: Comparison of S_1 energies for the acenes calculated using T-CDFT with PBE both when treated as pure HOMO \rightarrow LUMO excitations, and when treated as mixed excitations including all transition contributions greater than 0.01. Shown are the normalized transition contributions, as well as the calculated energies in eV.

	HOMO \rightarrow LUMO	HOMO-1 \rightarrow LUMO+1	HOMO-2 \rightarrow LUMO+2	Energy
naphthalene				
pure	1.000	-	-	4.33
mixed	0.935	0.027	0.038	4.41
anthracene				
pure	1.000	-	-	3.09
mixed	0.975	0.010	0.015	3.15
tetracene				
pure	1.000	-	-	2.29
mixed	0.988	0.012	-	2.32
pentacene				
pure	1.000	-	-	1.75
mixed	0.989	0.011	-	1.77
hexacene				
pure	1.000	-	-	1.35
mixed	0.989	0.011	-	1.37

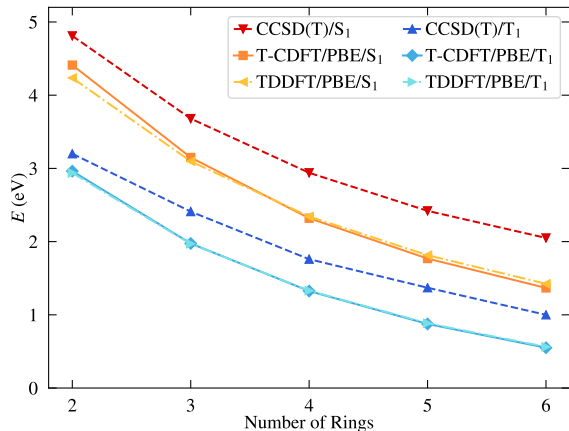


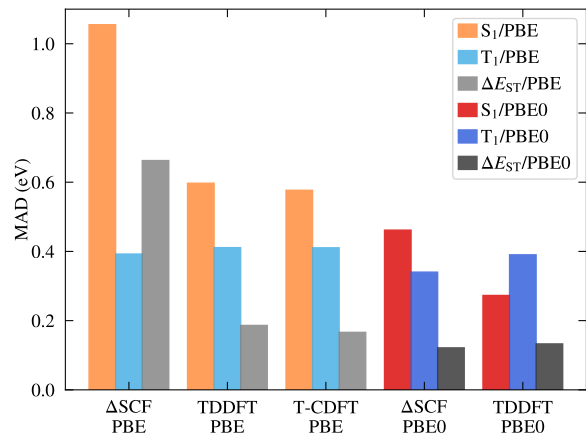
Figure 4: Trend in S_1 and T_1 energies for the acenes from naphthalene to hexacene, for both T-CDFT and TDDFT with PBE, as well as CCSD(T), where the latter values are taken from Ref.⁸².

(MAD) between each of the DFT-based approaches and CCSD(T). Compared to T_1 , S_1 is more sensitive to both method and functional, with T_1 energies being relatively consistent across the benchmark results, and in most cases having a smaller MAD than S_1 . Furthermore, the T-CDFT/PBE results are in remark-

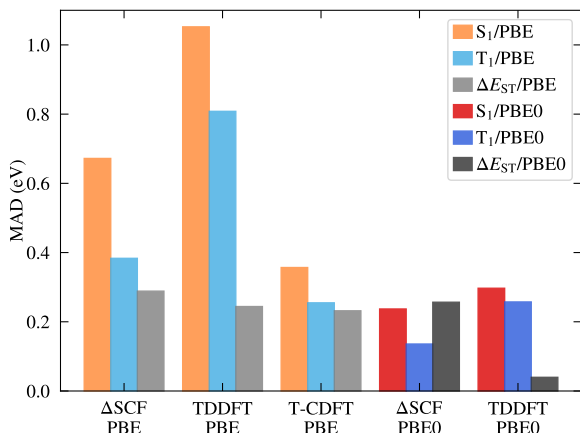
able agreement with TDDFT/PBE results despite the lower computational cost, with both approaches having MADs of 0.6 and 0.4 eV for S_1 and T_1 respectively. Both T-CDFT and TDDFT significantly outperform Δ SCF for S_1 when using PBE, while both Δ SCF and TDDFT with PBE0 give a modest improvement in accuracy, albeit at much higher computational cost. In short, we find that T-CDFT with PBE performs very well for the predominantly local excitations seen in the acenes.

3.3 OLEDs

Due to their larger size, there is a lack of higher level quantum chemical reference data for the OLED molecules. However, due to the CT-like nature of the excitations, TDDFT with semi-local functionals cannot be expected to provide a reasonable reference. Indeed, the limitations of TDDFT for CT states are well known, as is the corresponding strong dependence on the employed functional. This has motivated the use of range-separated hybrid functionals for the treatment of TADF materials.



(a) Acenes



(b) OLEDs

Figure 5: Mean absolute deviation (MAD) of benchmark vertical S_1 and T_1 energies for the set of molecules exhibiting pure excitations, relative to reference energies coming from CCSD(T)⁸² for the acenes and TDA-TDDFT with a tuned range-separated functional⁸⁴ for the OLEDs. Corresponding energies are given in the Supporting Information.

For example, Adachi and co-workers⁷⁸ reported that functionals such as CAM-B3LYP⁸⁵ or LC- ω PBE⁸⁶ tend to overestimate absorption energies for common TADF molecules. The situation may be improved by using “optimally” tuned range-separated functionals, which have been shown to give good agreement with experimental data^{84,87}, although the tuning of the separation parameters for a particular system increases the computational cost. Sun *et al.*⁸⁴ computed vertical excitation energies for a set of OLED molecules, including those considered

in this work, using TDA-TDDFT with an optimally tuned LC- ω PBE* functional and a 6-31+G(d) basis set. We use these values as a reference in the following, although we note that they were performed using an implicit solvent (PCM toluene), which may influence the results.

The MAD between our calculations and the reference values is depicted in Fig. 5(b). There is a greater variability in MADs across methods and functionals compared to the acenes, particularly for T_1 . Furthermore, both Δ SCF and TDDFT with PBE systematically underestimate the reference values (see Supporting Information), with the large MAD for TDDFT/PBE being particularly striking. On the other hand, T-CDFT/PBE performs significantly better, giving MADs which are closer to the Δ SCF and TDDFT PBE0 values. This much better performance of T-CDFT/PBE compared to TDDFT/PBE is in line with the more CT-like nature of the excitations. Indeed, TDDFT/PBE most strongly underestimates the excitation energies for the molecules with the strongest CT-like character (i.e. the smallest Λ_T values). At the same time, Fig. 6 shows that the smaller the value of Λ_T , the bigger the difference between T-CDFT/PBE and TDDFT/PBE. In other words, unlike TDDFT/PBE, which is strongly influenced by the nature of the transition, the quality of the T-CDFT/PBE results is not noticeably impacted by the nature of the excitation, giving reliable results for both the local excitations in acenes and the CT excitations in the OLED molecules.

Since accurate calculations of ΔE_{ST} are crucial for designing new, optimal TADF emitters, we conclude this section by discussing ΔE_{ST} . Both Δ SCF and TDDFT with PBE benefit to some degree from error cancellations in S_1 and T_1 errors, so that there is less variability across the methods. Nonetheless, while T-CDFT with PBE underestimates the reference ΔE_{ST} values, this is less severe than the PBE-calculated Δ SCF and TDDFT values. Furthermore, the MAD for T-CDFT/PBE is similar to that of Δ SCF with PBE0, and only outperformed by the significantly more expensive

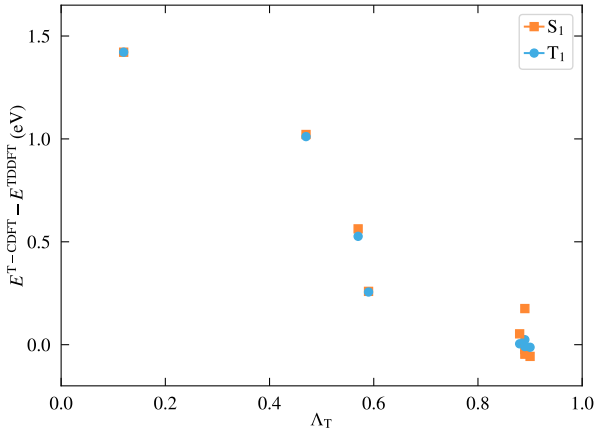


Figure 6: Difference between T-CDFT and TDDFT energies *vs.* Δ_T , the HOMO-LUMO spatial overlap, where both calculations employ the PBE functional.

TDDFT/PBE0 calculations.

To sum up, what emerges from our benchmark calculations and other computational works^{9,88,89} is that the modelling of the excitations in OLED molecules is strongly method- and functional- dependant, and it is therefore not trivial to obtain a unique and consistent description. Nonetheless, by comparing with tuned range-separated functional calculations, we see that, unlike TDDFT with PBE, T-CDFT is equally able to model both LE and CT states.

4 Conclusions

In this work we introduce a variation of CDFT (T-CDFT), wherein the constraint is defined as a transition between particular occupied and virtual orbitals, rather than a region of the simulation space as in traditional CDFT. By defining an approach which goes beyond the linear response regime, we aim to provide a tool for the robust modelling of excitations in molecules. Our approach is applied to acenes and OLED emitters, for which the lowest energy singlet and triplet states are dominated by a transition between the HOMO and LUMO. However, we also demonstrate the ability to take into account contributions from transitions between other orbitals. This has only a small impact on our benchmark calculations,

but could prove to be important in future investigations of excitations with a more strongly mixed character.

By comparing our benchmark calculations with reference values from the literature, we find that T-CDFT with PBE performs well for both the predominantly local excitations seen in the acenes, and the mix of CT and LE character seen in the OLED emitters, outperforming or equalling both Δ SCF and TDDFT with the same functional. Importantly, T-CDFT does not suffer from the problems encountered when applying TDDFT with semi-local functionals to CT states, and, unlike CDFT with a spatial constraint, can model both LE and CT states. At the same time, the computational cost of T-CDFT is similar to the ground state, while the ability to use a fixed (large) Lagrange multiplier keeps the cost significantly lower than TDDFT, even for mixed excitations involving multiple transitions. Furthermore, T-CDFT also proves to be more robust than Δ SCF, which can suffer from both spin contamination and convergence onto local minima.

Finally, our approach has been implemented in the linear scaling BigDFT code, and is fully compatible with the available fragmentation approaches. This capability could be used to impose excitations on a per-fragment basis in supramolecular or large biological systems. For example, in the case of local excitations on a molecule (fragment) in a given environment, where no strong coupling with the environment is expected, the constraint could be imposed between orbitals associated with the target fragment only, while still treating the *full system*. Such an approach has the advantage of screening out spurious low energy charge transfer excitations which can be encountered with TDDFT. On the other hand, in the case where charge transfer excitations between fragments are of interest, or where local excitations are expected to couple strongly with the environment, an alternative approach might be required. This could include performing TDDFT for a larger subset of the system, or using other information about the excitations to guide the choice of constraint(s). Crucially, our framework is flexible enough to impose both intra-

and inter-fragment constraints.

In summary, T-CDFT provides a robust and accurate approach for treating both LE and CT states. When combined with linear-scaling BigDFT, it is very well suited for treating excitations in large systems, enabling the exploration of explicit environmental effects on both excitation energies and ΔE_{ST} , a key quantity for modelling TADF-based OLEDs. Indeed, we foresee that such an approach will represent a powerful tool for the study of excitations in realistic supramolecular morphologies, for applications such as TADF. Work in this direction is ongoing.

Acknowledgement LER and MS acknowledge support from an EPSRC Early Career Research Fellowship (EP/P033253/1) and the Thomas Young Centre under grant number TYC-101. MS acknowledges Dr. Valerio Vitale for his initial help with automating the conversion between wavefunctions and support functions. KT acknowledges support from the Engineering and Physical Sciences Research Council (EP/S515085/1). Calculations were performed on the Imperial College High Performance Computing Service, the ARCHER UK National Supercomputing Service, and the ARCHER2 UK National Supercomputing Service (<https://www.archer2.ac.uk>). The Supporting Information contains additional computational details and further results. This includes a discussion of the investigation into local minima in ΔSCF , an example plot showing the effect of varying the Lagrange multiplier, a plot of the frontier orbital energies as calculated with PBE0, and tabulated data for the frontier orbital energies calculated using different basis sets, and both a plot and table containing the excitation energies calculated using the different approaches. In addition, the data associated with this work, including Jupyter notebooks and associated files which can be used to reproduce the calculations, are available at <https://gitlab.com/martistella86/t-cdft-notebooks>.

References

- (1) De Angelis, F. Modeling Materials and Processes in Hybrid/Organic Photovoltaics: From Dye-Sensitized to Perovskite Solar Cells. *Acc. Chem. Res.* **2014**, *47*, 3349–3360.
- (2) Tao, Y.; Yuan, K.; Chen, T.; Xu, P.; Li, H.; Chen, R.; Zheng, C.; Zhang, L.; Huang, W. Thermally Activated Delayed Fluorescence Materials Towards the Breakthrough of Organoelectronics. *Adv. Mater.* **2014**, *26*, 7931–7958.
- (3) Wong, M. Y.; Zysman-Colman, E. Purely Organic Thermally Activated Delayed Fluorescence Materials for Organic Light-Emitting Diodes. *Adv. Mater.* **2017**, *29*, 1605444.
- (4) Marques, M. A. L.; López, X.; Varsano, D.; Castro, A.; Rubio, A. Time-Dependent Density-Functional Approach for Biological Chromophores: The Case of the Green Fluorescent Protein. *Phys. Rev. Lett.* **2003**, *90*, 258101.
- (5) Carlson, S. A.; Hercules, D. M. Delayed Thermal Fluorescence of Anthraquinone in Solutions. *J. Am. Chem. Soc.* **1971**, *93*, 5611–5616.
- (6) Merkel, P. B.; Kearns, D. R. Oxygen Quenching and Radiationless Decay of Excited Singlet and Triplet State Carbonyl Compounds. *J. Chem. Phys.* **1973**, *58*, 398–400.
- (7) Hiroki, U.; Kenichi, G.; Katsuyuki, S.; Hiroko, N.; Chihaya, A. Highly Efficient Organic Light-Emitting Diodes From Delayed Fluorescence. *Nature* **2012**, *492*, 234–8.
- (8) Olivier, Y.; Yurash, B.; Muccioli, L.; D’Avino, G.; Mikhnenko, O.; Sancho-García, J. C.; Adachi, C.; Nguyen, T.-Q.; Beljonne, D. Nature of the Singlet and Triplet Excitations Mediating Thermally Activated Delayed Fluorescence. *Phys. Rev. Mat.* **2017**, *1*.

- (9) Olivier, Y.; Sancho-García, J.-C.; Muccioli, L.; D’Avino, G.; Beljonne, D. Computational Design of Thermally Activated Delayed Fluorescence Materials: The Challenges Ahead. *J. Phys. Chem. Lett* **2018**, *9*, 6149–6163.
- (10) Jacquemin, D.; Wathelet, V.; Perpète, E. A.; Adamo, C. Extensive TD-DFT Benchmark: Singlet-Excited States of Organic Molecules. *J. Chem. Theory Comput.* **2009**, *5*, 2420–2435.
- (11) van Setten, M. J.; Caruso, F.; Sharifzadeh, S.; Ren, X.; Scheffler, M.; Liu, F.; Lischner, J.; Lin, L.; Deslippe, J. R.; Louie, S. G.; Yang, C.; Weigend, F.; Neaton, J. B.; Evers, F.; Rinke, P. GW100: Benchmarking G0W0 for Molecular Systems. *J. Chem. Theory Comput.* **2015**, *11*, 5665–5687.
- (12) Hohenberg, P.; Kohn, W. Inhomogeneous Electron Gas. *Phys. Rev.* **1964**, *136*, B864–B871.
- (13) Kohn, W.; Sham, L. J. Self-Consistent Equations Including Exchange and Correlation Effects. *Phys. Rev.* **1965**, *140*, A1133–A1138.
- (14) Jones, R. O.; Gunnarsson, O. The Density Functional Formalism, its Applications and Prospects. *Rev. Mod. Phys.* **1989**, *61*, 689–746.
- (15) Gunnarsson, O.; Lundqvist, B. I. Exchange and Correlation in Atoms, Molecules, and Solids by the Spin-Density-Functional Formalism. *Phys. Rev. B* **1976**, *13*, 4274–4298.
- (16) Görling, A. Density-Functional Theory Beyond the Hohenberg-Kohn Theorem. *Phys. Rev. A* **1999**, *59*, 3359–3374.
- (17) Runge, E.; Gross, E. K. U. Density-Functional Theory for Time-Dependent Systems. *Phys. Rev. Lett.* **1984**, *52*, 997–1000.
- (18) Casida, M. E. *Recent Advances in Density Functional Methods*; 1995; pp 155–192.
- (19) Friesner, R. A. Ab Initio Quantum Chemistry: Methodology and Applications. *PNAS* **2005**, *102*, 6648–6653.
- (20) Liu, J.; Herbert, J. M. An Efficient and Accurate Approximation to Time-Dependent Density Functional Theory for Systems of Weakly Coupled Monomers. *J. Chem. Phys.* **2015**, *143*, 034106.
- (21) Zuehlsdorff, T. J.; Hine, N. D. M.; Payne, M. C.; Haynes, P. D. Linear-Scaling Time-Dependent Density-Functional Theory Beyond the Tamm-Dancoff Approximation: Obtaining Efficiency and Accuracy with in situ Optimised Local Orbitals. *J. Chem. Phys.* **2015**, *143*, 204107.
- (22) Isborn, C. M.; Götz, A. W.; Clark, M. A.; Walker, R. C.; Martinez, T. J. Electronic Absorption Spectra from MM and ab Initio QM/MM Molecular Dynamics: Environmental Effects on the Absorption Spectrum of Photoactive Yellow Protein. *J. Chem. Theory Comput.* **2012**, *8*, 5092–5106.
- (23) Neugebauer, J. Couplings between electronic transitions in a subsystem formulation of time-dependent density functional theory. *J. Chem. Phys.* **2007**, *126*, 134116.
- (24) Dreuw, A.; Head-Gordon, M. Failure of Time-Dependent Density Functional Theory for Long-Range Charge-Transfer Excited States: The Zinbacteriochlorin-Bacteriochlorin and Bacteriochlorophyll-Spheroidene Complexes. *J. Am. Chem. Soc.* **2004**, *126*, 4007–4016.
- (25) Kummel, S. Charge-Transfer Excitations: A Challenge for Time-Dependent Density Functional Theory That Has Been Met. *Adv. Energy Mater.* **2017**, *7*, 1700440.
- (26) Toulouse, J.; Colonna, F.; Savin, A. Long-range–Short-Range Separation of the

- Electron-Electron Interaction in Density-Functional Theory. *Phys. Rev. A* **2004**, *70*, 062505.
- (27) Dederichs, P. H.; Blügel, S.; Zeller, R.; Akai, H. Ground States of Constrained Systems: Application to Cerium Impurities. *Phys. Rev. Lett.* **1984**, *53*, 2512–2515.
- (28) Wu, Q.; Van Voorhis, T. Direct Optimization Method to Study Constrained Systems within Density-Functional Theory. *Phys. Rev. A* **2005**, *72*, 024502.
- (29) Kowalczyk, T.; Lin, Z.; Van Voorhis, T. Fluorescence Quenching by Photoinduced Electron Transfer in the Zn²⁺ Sensor Zinpyr-1: A Computational Investigation. *J. Phys. Chem. A* **2010**, *114*, 10427–10434.
- (30) Segal, M.; Singh, M.; Rivoire, K.; Difley, S.; Van Voorhis, T.; Baldo, M. A. Extrafluorescent Electroluminescence in Organic Light-Emitting Devices. *Nat. Mater.* **2007**, *6*, 374–378.
- (31) Difley, S.; Beljonne, D.; Van Voorhis, T. On the Singlet Triplet Splitting of Geminate Electron Hole Pairs in Organic Semiconductors. *J. Am. Chem. Soc.* **2008**, *130*, 3420–3427.
- (32) Sena, A. M. P.; Miyazaki, T.; Bowler, D. R. Linear Scaling Constrained Density Functional Theory in CONQUEST. *J. Chem. Theory Comput.* **2011**, *7*, 884–889.
- (33) Souza, A. M.; Rungger, I.; Pemmaraju, C. D.; Schwingenschloegl, U.; Sanvito, S. Constrained-DFT Method for Accurate Energy-Level Alignment of Metal/Molecule Interfaces. *Phys. Rev. B* **2013**, *88*, 165112.
- (34) Difley, S.; Van Voorhis, T. Exciton/Charge-Transfer Electronic Couplings in Organic Semiconductors. *J. Chem. Theory Comput.* **2011**, *7*, 594–601.
- (35) Roychoudhury, S.; Motta, C.; Sanvito, S. Charge Transfer Energies of Benzene Physisorbed on a Graphene Sheet from Constrained Density Functional Theory. *Phys. Rev. B* **2016**, *93*, 045130.
- (36) Kaduk, B.; Kowalczyk, T.; Van Voorhis, T. Constrained Density Functional Theory. *Chem. Rev.* **2012**, *112*, 321–370.
- (37) Ramos, P.; Pavanello, M. Constrained Subsystem Density Functional Theory. *Phys. Chem. Chem. Phys.* **2016**, *18*, 21172–21178.
- (38) Ramos, P.; Pavanello, M. Low-Lying Excited States by Constrained DFT. *J. Chem. Phys.* **2018**, *148*, 144103.
- (39) Roychoudhury, S.; O’Regan, D. D.; Teobaldi, G. Neutral Excitation Density-Functional Theory: an Efficient and Variational First-Principles Method for Simulating Neutral Excitations in Molecules. *Sci. Rep.* **2020**, *10*.
- (40) Evangelista, F. A.; Shushkov, P.; Tully, J. C. Orthogonality Constrained Density Functional Theory for Electronic Excited States. *J. Phys. Chem. A* **2013**, *117*, 7378–7392.
- (41) Senn, F.; Park, Y. C. Constricted Variational Density Functional Theory for Spatially Clearly Separated Charge-Transfer Excitations. *J. Chem. Phys.* **2016**, *145*, 244108.
- (42) Mohr, S.; Dawson, W.; Wagner, M.; Caliste, D.; Nakajima, T.; Genovese, L. Efficient Computation of Sparse Matrix Functions for Large-Scale Electronic Structure Calculations: The CheSS Library. *J. Chem. Theory Comput.* **2017**, *13*, 4684–4698.
- (43) Dawson, W.; Mohr, S.; Ratcliff, L. E.; Nakajima, T.; Genovese, L. Complexity Reduction in Density Functional Theory Calculations of Large Systems: System Partitioning and Fragment Embedding. *J.*

- Chem. Theory Comput.* **2020**, *16*, 2952–2964.
- (44) Ratcliff, L. E.; Dawson, W.; Fiscaro, G.; Caliste, D.; Mohr, S.; Degomme, A.; Videau, B.; Cristiglio, V.; Stella, M.; D’Alessandro, M.; Goedecker, S.; Nakajima, T.; Deutsch, T.; Genovese, L. Flexibilities of Wavelets as a Computational Basis Set for Large-Scale Electronic Structure Calculations. *J. Chem. Phys.* **2020**, *152*, 194110.
- (45) Mohr, S.; Ratcliff, L. E.; Boulanger, P.; Genovese, L.; Caliste, D.; Deutsch, T.; Goedecker, S. Daubechies Wavelets for Linear Scaling Density Functional Theory. *J. Chem. Phys.* **2014**, *140*.
- (46) Mohr, S.; Ratcliff, L. E.; Genovese, L.; Caliste, D.; Boulanger, P.; Goedecker, S.; Deutsch, T. Accurate and Efficient Linear Scaling DFT Calculations with Universal Applicability. *Phys. Chem. Chem. Phys.* **2015**, *17*, 31360–31370.
- (47) Rocca, D.; Gebauer, R.; Saad, Y.; Baroni, S. Turbo Charging Time-Dependent Density-Functional Theory with Lanczos Chains. *J. Chem. Phys.* **2008**, *128*, 154105.
- (48) D’Alessandro, M.; Genovese, L. Locality and Computational Reliability of Linear Response Calculations for Molecular Systems. *Phys. Rev. Materials* **2019**, *3*, 023805.
- (49) Jacquemin, D.; Perpète, E. A.; Scuseria, G. E.; Ciofini, I.; Adamo, C. TD-DFT Performance for the Visible Absorption Spectra of Organic Dyes: Conventional versus Long-Range Hybrids. *J. Chem. Theory Comput.* **2008**, *4*, 123–135.
- (50) Le Bahers, T.; Adamo, C.; Ciofini, I. A Qualitative Index of Spatial Extent in Charge-Transfer Excitations. *J. Chem. Theory Comput.* **2011**, *7*, 2498–2506.
- (51) Bedard-Hearn, M. J.; Sterpone, F.; Rossky, P. J. Nonadiabatic Simulations of Exciton Dissociation in Poly-p-phenylenevinylene Oligomers. *J. Phys. Chem. A* **2010**, *114*, 7661–7670.
- (52) Nitta, H.; Kawata, I. A Close Inspection of the Charge-Transfer Excitation by TDDFT with Various Functionals: An Application of Orbital- and Density-Based Analyses. *Chem. Phys.* **2012**, *405*, 93–99.
- (53) Peach, M. J. G.; Benfield, P.; Helgaker, T.; Tozer, D. J. Excitation Energies in Density Functional Theory: An Evaluation and a Diagnostic Test. *J. Chem. Phys.* **2008**, *128*, 044118.
- (54) Plasser, F.; Lischka, H. Analysis of Excitonic and Charge Transfer Interactions from Quantum Chemical Calculations. *J. Chem. Theory Comput.* **2012**, *8*, 2777–2789.
- (55) Guido, C. A.; Cortona, P.; Mennucci, B.; Adamo, C. On the Metric of Charge Transfer Molecular Excitations: A Simple Chemical Descriptor. *J. Chem. Theory Comput.* **2013**, *9*, 3118–3126.
- (56) Daubechies, I. *Ten Lectures on Wavelets*; SIAM, 1992.
- (57) Genovese, L.; Neelov, A.; Goedecker, S.; Deutsch, T.; Ghasemi, S. A.; Willand, A.; Caliste, D.; Zilberberg, O.; Rayson, M.; Bergman, A.; Schneider, R. Daubechies Wavelets as a Basis Set for Density Functional Pseudopotential Calculations. *J. Chem. Phys.* **2008**, *129*, 014109.
- (58) Ratcliff, L. E.; Genovese, L.; Mohr, S.; Deutsch, T. Fragment Approach to Constrained Density Functional Theory Calculations using Daubechies Wavelets. *J. Chem. Phys.* **2015**, *142*, –.
- (59) Ratcliff, L. E.; Grisanti, L.; Genovese, L.; Deutsch, T.; Neumann, T.; Danilov, D.; Wenzel, W.; Beljonne, D.; Cornil, J. Toward Fast and Accurate Evaluation of

- Charge On-Site Energies and Transfer Integrals in Supramolecular Architectures Using Linear Constrained Density Functional Theory (CDFT)-Based Methods. *J. Chem. Theory Comput.* **2015**, *11*, 2077–2086.
- (60) Hernández, E.; Gillan, M. J. Self-Consistent First-Principles Technique with Linear Scaling. *Phys. Rev. B* **1995**, *51*, 10157–10160.
- (61) Kohn, W. Density Functional and Density Matrix Method Scaling Linearly with the Number of Atoms. *Phys. Rev. Lett.* **1996**, *76*, 3168–3171.
- (62) Goedecker, S.; Colombo, L. Efficient Linear Scaling Algorithm for Tight-Binding Molecular Dynamics. *Phys. Rev. Lett.* **1994**, *73*, 122–125.
- (63) Goedecker, S.; Teter, M. Tight-Binding Electronic-Structure Calculations and Tight-Binding Molecular Dynamics with Localized Orbitals. *Phys. Rev. B* **1995**, *51*, 9455–9464.
- (64) Ratcliff, L. E.; Genovese, L. Pseudo-Fragment Approach for Extended Systems Derived from Linear-Scaling DFT. *J. Phys.: Condens. Matter* **2019**, *31*, 285901.
- (65) Mohr, S.; Masella, M.; Ratcliff, L. E.; Genovese, L. Complexity Reduction in Large Quantum Systems: Fragment Identification and Population Analysis via a Local Optimized Minimal Basis. *J. Chem. Theory Comput.* **2017**, *13*, 4079–4088.
- (66) Prentice, J. C. A. et al. The ONETEP Linear-Scaling Density Functional Theory Program. *J. Chem. Phys.* **2020**, *152*, 174111.
- (67) Skylaris, C.-K.; Haynes, P. D.; Mostofi, A. A.; Payne, M. C. Introducing ONETEP: Linear-Scaling Density Functional Simulations on Parallel Computers. *J. Chem. Phys.* **2005**, *122*, 84119.
- (68) Ratcliff, L. E.; Hine, N. D. M.; Haynes, P. D. Calculating Optical Absorption Spectra for Large Systems Using Linear-Scaling Density Functional Theory. *Phys. Rev. B* **2011**, *84*, 165131.
- (69) Perdew, J. P.; Burke, K.; Ernzerhof, M. Generalized Gradient Approximation Made Simple. *Phys. Rev. Lett.* **1996**, *77*, 3865–3868.
- (70) Adamo, C.; Barone, V. Toward Reliable Density Functional Methods Without Adjustable Parameters: The PBE0 Model. *J. Chem. Phys.* **1999**, *110*, 6158–6170.
- (71) Kowalczyk, T.; Yost, S. R.; Voorhis, T. V. Assessment of the Δ SCF Density Functional Theory Approach for Electronic Excitations in Organic Dyes. *J. Chem. Phys.* **2011**, *134*, 054128.
- (72) Valiev, M.; Bylaska, E.; Govind, N.; Kowalski, K.; Straatsma, T.; Van Dam, H.; Wang, D.; Nieplocha, J.; Apra, E.; Windus, T.; de Jong, W. NWChem: A Comprehensive and Scalable Open-Source Solution for Large Scale Molecular Simulations. *Comput. Phys. Commun.* **2010**, *181*, 1477 – 1489.
- (73) Peach, M. J.; Warner, N.; Tozer, D. J. On the Triplet Instability in TDDFT. *Mol. Phys.* **2013**, *111*, 1271–1274.
- (74) Dunning, T. H. Gaussian Basis Sets for Use in Correlated Molecular Calculations. I. The Atoms Boron through Neon and Hydrogen. *J. Chem. Phys.* **1989**, *90*, 1007–1023.
- (75) Ceperley, D. M.; Alder, B. J. Ground State of the Electron Gas by a Stochastic Method. *Phys. Rev. Lett.* **1980**, *45*, 566–569.
- (76) Yang, Z.; Mao, Z.; Xie, Z.; Zhang, Y.; Liu, S.; Zhao, J.; Xu, J.; Chi, Z.; Aldred, M. P. Recent Advances in Organic Thermally Activated Delayed Fluorescence Materials. *Chem. Soc. Rev.* **2017**, *46*, 915–1016.

- (77) Hait, D.; Zhu, T.; McMahon, D. P.; Van Voorhis, T. Prediction of Excited-State Energies and Singlet-Triplet Gaps of Charge-Transfer States Using a Restricted Open-Shell Kohn-Sham Approach. *J. Chem. Theory Comput.* **2016**, *12*, 3353–3359.
- (78) Huang, S.; Zhang, Q.; Shiota, Y.; Nakagawa, T.; Kuwabara, K.; Yoshizawa, K.; Adachi, C. Computational Prediction for Singlet- and Triplet-Transition Energies of Charge-Transfer Compounds. *J. Chem. Theory Comput.* **2013**, *9*, 3872–3877.
- (79) Yang, Y.; Davidson, E. R.; Yang, W. Nature of Ground and Electronic Excited States of Higher Acenes. *PNAS* **2016**, *113*, E5098–E5107.
- (80) Momma, K.; Izumi, F. *VESTA3* for Three-Dimensional Visualization of Crystal, Volumetric and Morphology Data. *J. Appl. Crystallogr.* **2011**, *44*, 1272–1276.
- (81) Bertels, L. W.; Lee, J.; Head-Gordon, M. Polishing the Gold Standard: The Role of Orbital Choice in CCSD(T) Vibrational Frequency Prediction. *J. Chem. Theory Comput.* **2021**, *17*, 742–755.
- (82) Rangel, T.; Hamed, S. M.; Bruneval, F.; Neaton, J. B. An Assessment of Low-Lying Excitation Energies and Triplet Instabilities of Organic Molecules with an Ab Initio Bethe-Salpeter Equation Approach and the Tamm-Dancoff Approximation. *J. Chem. Phys.* **2017**, *146*, 194108.
- (83) Platt, J. R. Classification of Spectra of Cata-Condensed Hydrocarbons. *J. Chem. Phys.* **1949**, *17*, 484–495.
- (84) Sun, H.; Zhong, C.; Brédas, J.-L. Reliable Prediction with Tuned Range-Separated Functionals of the Singlet-Triplet Gap in Organic Emitters for Thermally Activated Delayed Fluorescence. *J. Chem. Theory Comput.* **2015**, *11*, 3851–3858.
- (85) A New Hybrid Exchange-Correlation Functional Using the Coulomb-Attenuating Method (CAMB3LYP). *Chem. Phys. Lett.* **2004**, *393*, 51–57.
- (86) Vydrov, O. A.; Scuseria, G. E. Assessment of a Long-Range Corrected Hybrid Functional. *J. Chem. Phys.* **2006**, *125*, 234109.
- (87) Penfold, T. J. On Predicting the Excited-State Properties of Thermally Activated Delayed Fluorescence Emitters. *J. Phys. Chem. C* **2015**, *119*, 13535–13544.
- (88) Moral, M.; Muccioli, L.; Son, W.-J.; Olivier, Y.; Sancho-García, J. C. Theoretical Rationalization of the Singlet-Triplet Gap in OLEDs Materials: Impact of Charge-Transfer Character. *J. Chem. Theory Comput.* **2015**, *11*, 168–177.
- (89) Sanz-Rodrigo, J.; Olivier, Y.; Sancho-García, J.-C. Computational Studies of Molecular Materials for Unconventional Energy Conversion: The Challenge of Light Emission by Thermally Activated Delayed Fluorescence. *Molecules* **2020**, *25*, 1006.

Supplementary Information

Transition-Based Constrained DFT for the Robust and Reliable Treatment of Excitations in Supramolecular Systems

Martina Stella,^{1,2} Kritam Thapa,¹ Luigi Genovese,³ and Laura E. Ratcliff^{1,4}

¹*Department of Materials, Imperial College London, London SW7 2AZ, United Kingdom*

²*The Abdus Salam International Centre for Theoretical Physics, Condensed Matter and Statistical Physics, 34151 Trieste, Italy*

³*Univ. Grenoble Alpes, CEA, IRIG-MEM-L-Sim, 38000 Grenoble, France*

⁴*Centre for Computational Chemistry, School of Chemistry, University of Bristol, Bristol BS8 1TS, United Kingdom*

(Dated: March 10, 2022)

A. Additional Computational Details

BigDFT calculations were performed using HGH-GTH PSPs^{1,2} with non-linear core corrections.³ Gas phase geometry optimizations were performed for the ground state using PBE in BigDFT, with a maximum force threshold of 0.02 eV/Å. Single point calculations were performed with a wavelet grid spacing of 0.26 Å, while geometry optimizations employed a smaller grid spacing of 0.24 Å to ensure accurate force calculations. All BigDFT calculations used coarse and fine multipliers of 7 and 9 respectively. Cubic scaling BigDFT calculations employed a gradient convergence threshold of 10^{-5} . Due to the poor convergence behaviour of some NWChem calculations, a strict upper limit of 200 iterations was imposed for both Δ SCF and TDDFT calculations, beyond which calculations were considered not to have reached convergence.

T-CDFT WFN-based calculations were performed for a range of basis sizes, while SF-based calculations were performed for a range of localization radii for two basis set sizes – a minimal basis with 1/4/4 basis functions per H/C/N atom and a larger basis with 4/9/9 basis functions per H/C/N atom. The minimal basis was insufficient, giving energies almost 0.2 eV higher in energy than the more converged basis. On the other hand, increasing the localization radius from 4.23 to 5.29 Å led to differences less than 0.05 eV. We note that, due to the presence of additional degrees of freedom coming from environment molecules, it may be possible to use a smaller SF basis while retaining the same accuracy in future T-CDFT calculations of larger systems. All SF-based T-CDFT calculations were performed for a basis set optimized to represent all negative energy (bound) virtual states, as identified from the equivalent cubic scaling PBE calculation. No kernel truncation was applied, since the addition of the constraint decreases the locality of the kernel.

The HOMO-LUMO spatial overlap, Λ_T , was calculated as a post-processing calculation using the HOMO and LUMO wavefunctions extracted from cubic-scaling BigDFT. The HOMO-LUMO transition purity, \mathcal{P} , or the full transition breakdown in the case of mixed excitations, was also calculated as a post-processing step following BigDFT TDDFT calculations with LDA in a PBE-generated WFN basis, for which care was also taken to ensure the basis set contained enough virtual states to reach convergence. Although not used in this work, the functionality also exists to calculate transition purities using a SF basis.

B. Local Minima in Δ SCF

For calculations which were performed using both BigDFT and NWChem, a close comparison of results was performed. In general, the results showed good agreement, however there were some large deviations between Δ SCF values between the two codes, which could not be attributed to basis set differences or the use of pseudopotentials, even when accounting for the fact that purification increases uncertainties in S_1 coming from basis set, PSP and convergence differences. Indeed, although generally considered a reliable tool for the computation of vertical HOMO-LUMO transitions in organic emitters,⁴ because SCF algorithms are geared toward energy minimization, Δ SCF is known to sometimes collapse to low energy states. This can include the ground state,⁵ although methods such as the maximum overlap method⁶ have been developed to alleviate this problem. For some OLED molecules, it has also been observed to converge onto a different excited state due to a poor orbital guess or degeneracy.⁷

In this work no collapses onto the ground state were observed. However, large initial variations between BigDFT and NWChem energies were found, which could not be explained by basis set differences, even taking into account the fact that the use of the purification formula can exaggerate differences in singlet energies if the triplet states also differ. Instead, the variations were attributed to the presence of local minima, which was confirmed by inspecting the charge density differences between the ground state and the corresponding excited state. It was found that using the

ground state orbitals as an initial guess for excited state calculations eliminated these local minima, typically also improving convergence. This was confirmed by again inspecting the charge density differences.

C. Lagrange Multiplier

Fig. S1 shows the effect of varying the Lagrange multiplier for a pure excitation in naphthalene. A value of -20 was used in all calculations, giving $\text{Tr}(\mathbf{KW})$ within 0.01 of $1e^-$ and thus confirming that there is no need to optimize V_c on a case-by-case basis.

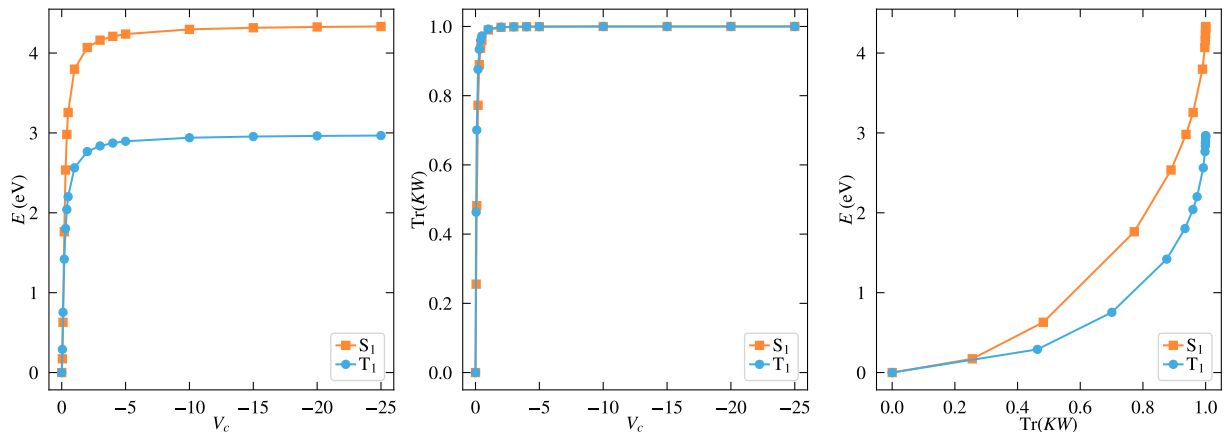


FIG. S1: Influence of the Lagrange multiplier, V_c , on the T-CDFT calculated singlet and triplet energies for a pure HOMO-LUMO constraint in naphthalene, as well as the constrained charge, $\text{Tr}(KW)$, and the relation between the two. Calculations are performed for a SF basis with 4(9) SFs per H(C) atom, with localization radii $R_{\text{loc}} = 4.23 \text{ \AA}$.

D. Additional Results

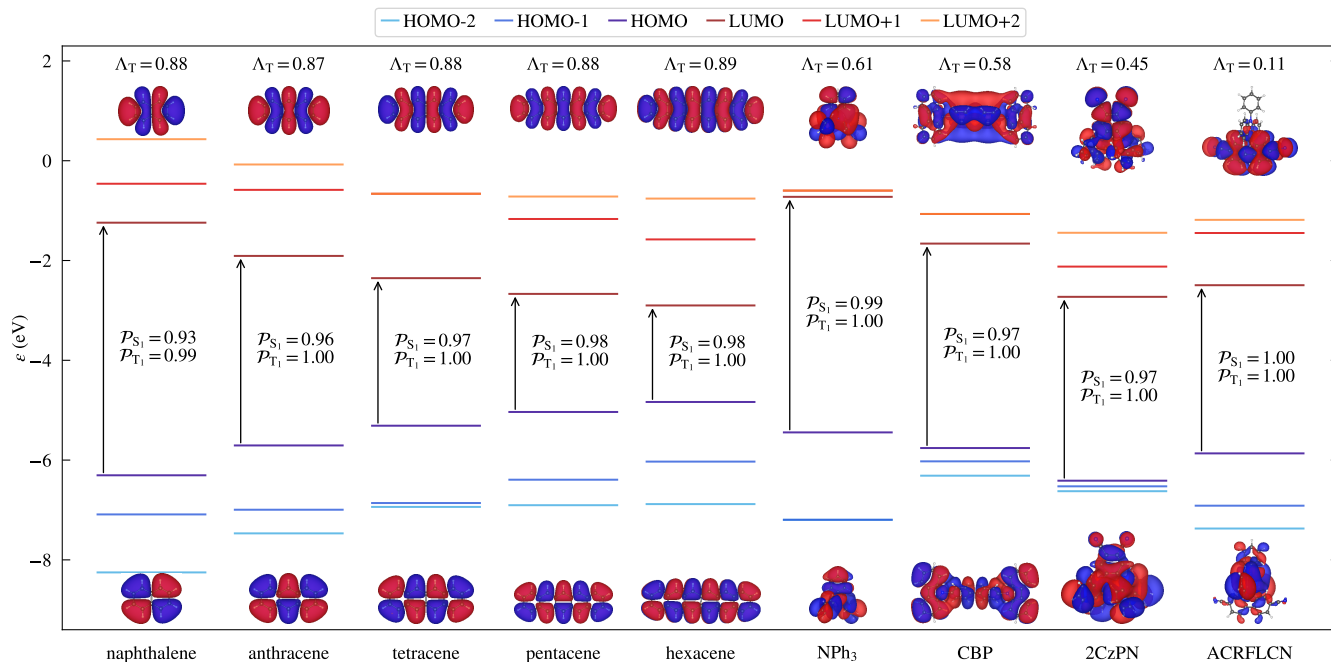


FIG. S2: PBE0-calculated frontier orbital energies and corresponding HOMO and LUMO wavefunctions, as obtained from NWChem using the cc-pVTZ basis. Wavefunctions were visualized in VESTA, using an isosurface value of $0.0005 a_0^{-3/2}$. The corresponding charge transfer parameter, Λ_T and HOMO-LUMO transition purity values, \mathcal{P} , are also given for each molecule, where the latter are calculated using LDA with a PBE basis, as described in the main text. The corresponding energies are given in Tables S1 and S2.

TABLE S1: Frontier orbital energies and band gaps of the acenes, calculated using different functionals with the cc-pVTZ ('VTZ') basis set in NWChem, a wavelet basis using the cubic scaling approach of BigDFT and a SF basis of 4/9/9 SFs per H/C/N atom with $R_{loc} = 4.23$ Å. All values are in eV.

	PBE			PBE0	
	VTZ	wavelet	SF	VTZ	wavelet
naphthalene					
HOMO-2	-7.11	-7.15	-7.16	-8.23	-8.25
HOMO-1	-6.18	-6.22	-6.23	-7.07	-7.09
HOMO	-5.45	-5.48	-5.50	-6.30	-6.30
LUMO	-2.04	-2.09	-2.09	-1.22	-1.24
LUMO+1	-1.28	-1.34	-1.30	-0.43	-0.46
LUMO+2	-0.43	-0.56	-0.45	0.59	0.43
gap	3.40	3.39	3.41	5.07	5.06
anthracene					
HOMO-2	-6.44	-6.47	-6.48	-7.46	-7.47
HOMO-1	-6.14	-6.17	-6.18	-6.98	-6.99
HOMO	-4.95	-4.98	-5.00	-5.70	-5.71
LUMO	-2.63	-2.67	-2.67	-1.90	-1.91
LUMO+1	-1.37	-1.42	-1.38	-0.57	-0.58
LUMO+2	-1.00	-1.07	-1.03	-0.03	-0.08
gap	2.32	2.32	2.33	3.80	3.80
tetracene					
HOMO-2	-6.11	-6.15	-6.16	-6.93	-6.94
HOMO-1	-5.92	-5.95	-5.97	-6.86	-6.86
HOMO	-4.63	-4.66	-4.67	-5.31	-5.31
LUMO	-3.00	-3.04	-3.05	-2.35	-2.35
LUMO+1	-1.55	-1.60	-1.59	-0.65	-0.66
LUMO+2	-1.42	-1.46	-1.46	-0.65	-0.66
gap	1.62	1.62	1.62	2.96	2.96
pentacene					
HOMO-2	-6.10	-6.13	-6.15	-6.90	-6.90
HOMO-1	-5.53	-5.56	-5.58	-6.39	-6.39
HOMO	-4.41	-4.44	-4.45	-5.04	-5.04
LUMO	-3.27	-3.30	-3.31	-2.67	-2.67
LUMO+1	-2.00	-2.03	-2.04	-1.17	-1.17
LUMO+2	-1.46	-1.50	-1.49	-0.72	-0.72
gap	1.14	1.14	1.14	2.37	2.37
hexacene					
HOMO-2	-6.10	-6.12	-6.14	-6.88	-6.88
HOMO-1	-5.23	-5.26	-5.27	-6.03	-6.03
HOMO	-4.25	-4.28	-4.29	-4.85	-4.84
LUMO	-3.46	-3.48	-3.49	-2.90	-2.90
LUMO+1	-2.35	-2.38	-2.39	-1.58	-1.58
LUMO+2	-1.49	-1.52	-1.51	-0.76	-0.76
gap	0.79	0.80	0.80	1.94	1.93

TABLE S2: Frontier orbital energies and band gaps of the OLED molecules, calculated using different functionals with the cc-pVTZ ('VTZ') basis set in NWChem, a wavelet basis using the cubic scaling approach of BigDFT and a SF basis of 4/9/9 SFs per H/C/N atom with $R_{\text{loc}} = 4.23 \text{ \AA}$. All values are in eV.

	PBE			PBE0	
	VTZ	wavelet	SF	VTZ	wavelet
NPh3					
HOMO-2	-6.20	-6.24	-6.28	-7.18	-7.20
HOMO-1	-6.20	-6.24	-6.28	-7.18	-7.20
HOMO	-4.57	-4.61	-4.65	-5.43	-5.45
LUMO	-1.53	-1.60	-1.60	-0.67	-0.72
LUMO+1	-1.43	-1.50	-1.51	-0.55	-0.60
LUMO+2	-1.43	-1.49	-1.51	-0.55	-0.60
gap	3.04	3.01	3.05	4.77	4.72
CBP					
HOMO-2	-5.46	-5.50	-5.52	-6.31	-6.31
HOMO-1	-5.14	-5.17	-5.20	-6.01	-6.03
HOMO	-4.92	-4.96	-4.99	-5.75	-5.76
LUMO	-2.41	-2.46	-2.47	-1.65	-1.66
LUMO+1	-1.86	-1.92	-1.91	-1.04	-1.07
LUMO+2	-1.82	-1.88	-1.88	-1.04	-1.07
gap	2.51	2.50	2.52	4.11	4.10
2CzPN					
HOMO-2	-5.78	-5.82	-5.85	-6.59	-6.62
HOMO-1	-5.63	-5.67	-5.70	-6.49	-6.53
HOMO	-5.54	-5.58	-5.61	-6.38	-6.41
LUMO	-3.43	-3.48	-3.50	-2.70	-2.73
LUMO+1	-2.93	-2.99	-3.01	-2.08	-2.12
LUMO+2	-2.20	-2.26	-2.27	-1.39	-1.44
gap	2.11	2.10	2.11	3.68	3.69
ACRFLCN					
HOMO-2	-6.34	-6.38	-6.40	-7.35	-7.37
HOMO-1	-6.03	-6.07	-6.09	-6.90	-6.91
HOMO	-4.95	-5.00	-5.02	-5.85	-5.87
LUMO	-3.17	-3.22	-3.23	-2.48	-2.49
LUMO+1	-2.26	-2.33	-2.32	-1.40	-1.45
LUMO+2	-2.01	-2.07	-2.07	-1.16	-1.19
gap	1.79	1.78	1.79	3.37	3.37

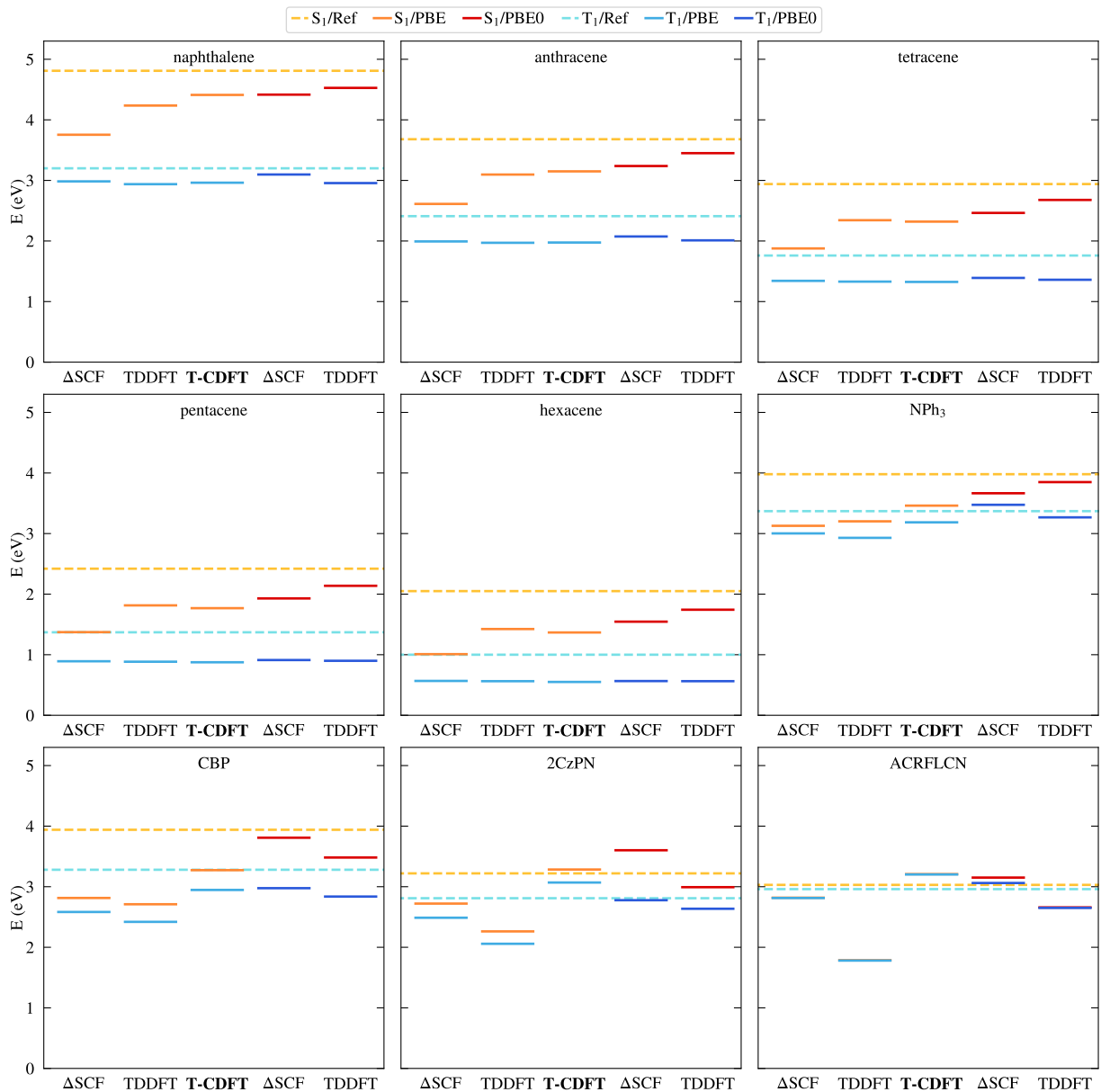


FIG. S3: Vertical S_1 and T_1 energies computed using different methods (T-CDFT, Δ SCF, TDDFT) and functionals (PBE, PBE0) using BigDFT and NWChem. Corresponding energies are given in Table S3, while the reference energies are calculated using CCSD(T)^{8,9} for the acenes, and TDA-TDDFT with a tuned range-separated functional¹⁰ for the OLEDs.

TABLE S3: Vertical S_1 and T_1 energies and singlet-triplet splittings, ΔE_{ST} , in eV, calculated using different methods (T-CDFT, Δ SCF, TDDFT) and functionals (PBE, PBE0) using BigDFT and NWChem, as compared to reference values from CCSD(T)^{8,9} for the acenes, and TDA-TDDFT with a tuned range-separated functional¹⁰ for the OLEDs. Also given is the HOMO-LUMO transition purity, \mathcal{P} , the spatial overlap, Λ_T , and the mean absolute deviation (MAD) of the different quantities with respect to the reference values.

	Ref	\mathcal{P}	PBE			PBE0			
			Λ_T	Δ SCF	TDDFT	T-CDFT	Λ_T	Δ SCF	TDDFT
naphthalene									
S_1	4.81	0.93		3.75	4.24	4.41		4.42	4.53
T_1	3.20	0.99	0.89	2.98	2.94	2.96	0.88	3.10	2.96
ΔE_{ST}	1.61			0.77	1.30	1.36		1.32	1.57
anthracene									
S_1	3.68	0.96		2.61	3.10	3.15		3.24	3.45
T_1	2.41	1.00	0.88	1.99	1.97	1.97	0.87	2.07	2.01
ΔE_{ST}	1.27			0.62	1.13	1.12		1.16	1.44
tetracene									
S_1	2.94	0.97		1.88	2.34	2.32		2.46	2.68
T_1	1.76	1.00	0.89	1.34	1.33	1.32	0.88	1.39	1.36
ΔE_{ST}	1.18			0.54	1.01	0.97		1.07	1.32
pentacene									
S_1	2.42	0.98		1.37	1.81	1.75		1.93	2.14
T_1	1.37	1.00	0.89	0.89	0.88	0.88	0.88	0.91	0.90
ΔE_{ST}	1.05			0.48	0.93	0.87		1.02	1.24
hexacene									
S_1	2.05	0.98		1.01	1.42	1.37		1.55	1.74
T_1	1.00	1.00	0.90	0.57	0.56	0.55	0.89	0.56	0.56
ΔE_{ST}	1.05			0.44	0.86	0.80		0.98	1.18
MAD									
S_1				1.06	0.60	0.58		0.46	0.27
T_1				0.39	0.41	0.41		0.34	0.39
ΔE_{ST}				0.66	0.19	0.17		0.12	0.13
NPh₃									
S_1	3.98	0.99		3.13	3.20	3.46		3.67	3.85
T_1	3.37	1.00	0.59	3.00	2.93	3.19	0.61	3.47	3.27
ΔE_{ST}	0.61			0.13	0.27	0.28		0.19	0.58
CBP									
S_1	3.94	0.97		2.81	2.71	3.27		3.81	3.48
T_1	3.28	1.00	0.57	2.58	2.42	2.95	0.58	2.98	2.84
ΔE_{ST}	0.66			0.23	0.29	0.33		0.83	0.64
2CzPN									
S_1	3.22	0.97		2.72	2.26	3.28		3.60	2.99
T_1	2.81	1.00	0.47	2.49	2.06	3.07	0.45	2.78	2.64
ΔE_{ST}	0.41			0.23	0.20	0.21		0.82	0.36
ACRFLCN									
S_1	3.03	1.00		2.82	1.79	3.21		3.15	2.66
T_1	2.96	1.00	0.12	2.81	1.78	3.20	0.11	3.06	2.65
ΔE_{ST}	0.07			0.01	0.01	0.01		0.09	0.01
MAD									
S_1				0.67	1.05	0.36		0.24	0.30
T_1				0.38	0.81	0.25		0.14	0.26
ΔE_{ST}				0.29	0.24	0.23		0.26	0.04

-
- ¹ S. Goedecker, M. Teter, and J. Hutter, *Phys. Rev. B* **54**, 1703 (1996).
 - ² C. Hartwigsen, S. Goedecker, and J. Hutter, *Phys. Rev. B* **58**, 3641 (1998).
 - ³ A. Willand, Y. O. Kvashnin, L. Genovese, A. Vázquez-Mayagoitia, A. K. Deb, A. Sadeghi, T. Deutsch, and S. Goedecker, *J. Chem. Phys.* **138**, 104109 (2013).
 - ⁴ T. Kowalczyk, S. R. Yost, and T. V. Voorhis, *J. Chem. Phys.* **134**, 054128 (2011).
 - ⁵ S. Bourne Worster, O. Feighan, and F. R. Manby, *J. Chem. Phys.* **154**, 124106 (2021).
 - ⁶ A. T. B. Gilbert, N. A. Besley, and P. M. W. Gill, *J. Phys. Chem. A* **112**, 13164 (2008).
 - ⁷ K. Zhao, Ö. H. Omar, T. Nemataram, D. Padula, and A. Troisi, *J. Mater. Chem. C* **9**, 3324 (2021).
 - ⁸ T. Rangel, S. M. Hamed, F. Bruneval, and J. B. Neaton, *J. Chem. Phys.* **146**, 194108 (2017).
 - ⁹ K. Lopata, R. Reslan, M. Kowalska, D. Neuhauser, N. Govind, and K. Kowalski, *J. Chem. Theory Comput.* **7**, 3686 (2011).
 - ¹⁰ H. Sun, C. Zhong, and J.-L. Brédas, *J. Chem. Theory Comput.* **11**, 3851 (2015).